New Insights into the Electrochemistry of Molybdenum(VI) Dioxo Complexes Containing a Tetradentate $S_2(NH)_2$-Type Ligand

Ulrich Küsthardt,* Rolf W. Albach, and Paul Kiprof

Anorganisch-Chemisches Institut der Technischen Universität München, Lichtenbergstrasse 4, D-8046 Garching, Germany

Received August 20, 1992

The electrochemistry of dioxomolybdenum(VI) with the tetradentate $S_2(NH)_2$-type ligand N,N′-bis(2-mercaptophenyl)-2,3-diaminobutane ($mPhabH_4$), at neutral, acidic, and basic conditions, has been investigated. The molecular structure of $(mPhabH_2)Mo^{VI}O_2$ (**1**) has been determined: space group $P2_12_12_1$ (No. 19), a = 8.667(<1), b = 12.884(<1), c = 19.877(3) Å, V = 2220 Å^3; Z = 4. The cis-dioxo complex **1** displays a highly distorted octahedral structure. Electrochemical, one-electron reduction of the Mo(VI) compound **1** is followed by a fast dehydration reaction leading to $[(mPhab)MoO]^-$ (**4**), which can be further reduced in a subsequent one-electron reduction step to the Mo(IV) dianion. At neutral conditions this process appears as a single two-electron reduction. Upon addition of *N*-methylimidazole (NMI) the dehydration rate decreases and two separate reduction steps can be observed. Acidic conditions also lead to a decrease of the dehydration rate and to two separate one-electron reductions. In basic solution the Mo(VI) complex **1** is reduced by methanol to $[(mPhab)Mo^{V}O]^-$ (**4**), which shows both a quasi-reversible one-electron reduction wave to form the Mo(IV) dianion and a quasi-reversible oxidation wave. Synthetically, $[(mPhab)Mo^{V}O]^-$ (**4**) can also be obtained via deoxygenation of **1** by Ph_2PMe in the presence of *N*-methylimidazole, presumably via formation of a Mo(IV)–NMI adduct that undergoes a comproportionation reaction with **1** and subsequent dehydration to the mononuclear Mo(V) complex **4**. Neither μ-oxo-bridged Mo(V) dimers nor mononuclear Mo(IV) species can be detected.

Introduction

Molybdenum is an essential second row transition metal element in the active site of many hydroxylases that catalyze two-electron redox processes.[1] All oxo–molybdoenzymes depend on a common molybdenum cofactor (Mo-co),[2] and the molybdenum centers are thought to cycle between Mo(VI), Mo(V), and Mo(IV) during the catalytic cycle. A basic feature of the reactions catalyzed by Mo-co is that they all formally involve the transfer of an oxygen atom to or from a substrate molecule. A second center is required as an electron acceptor (oxidases) or electron donor (reductases). Heme centers, Fe–S cluster centers, and sometimes flavins serve this electron acceptor (donor) function. Therefore the molybdenum center acts as a relay station between a two-electron substrate redox reaction and two coupled one-electron redox reactions at the other electron-transfer center.

The redox reaction of the substrate can be described as an oxo-transfer reaction or alternatively as a coupled electron/proton transfer (2 e^-/2 H^+) reaction.[3] The latter proceeds in the case of sulfite oxidase (MoO_2^{2+}) via $MoO(OH)^{2+}$ species, as suggested by EPR studies.[4]

To date, electrochemical studies on hydroxylases are limited to coulometric (equilibrium state) studies.[5] Nonequilibrium, fast methods like cyclovoltammetry[6] (CV) have not been successfully applied to molybdoenzymes. In contrast, a vast number of cyclovoltammetric studies on molybdenum model compounds containing tetradentate S_2N_2 ligands are known.[7-11] However, most of these previous studies were performed at neutral conditions. Here we show that the electrochemistry of a synthetically known Mo(VI)–dioxo[12] compound containing a tetradentate $(NH)_2S_2$ ligand is strongly dependent upon pH. On the basis of our electrochemical results at low, neutral, and high proton concentrations, we propose requirements for the ligand sphere at the active site (Mo-co) of molybdenum-containing hydroxylases.

Experimental Section

Syntheses. All syntheses were performed under a nitrogen or argon atmosphere by using standard Schlenk techniques.[13] All solvents were dried and distilled before use.[14] Satisfactory elemental analyses were obtained for all described complexes.

$(mPhabH_2)MoO_2$. The synthesis of the complex $(mPhabH_2)MoO_2$ was based upon published procedures.[12,15,16] However, modifications have been made to increase yields and simplify the synthetic route. The modified procedures are listed below.

We found that the required amounts of DMF have to be significantly reduced for the reduction of (1,4-diaza-*N*,*N*′-(2-mercaptophenyl)-2,3-methyl-1,3-butadienato)zinc (dmPhb)Zn to give $(mPhabH_2)Zn$: 1.7 mL of a 1.6 M solution of $NaBH_4$ (2.7 mmol) in DMF was added dropwise

(1) Rajagopalan, K. V. *Nutr. Rev.* **1987**, *45*, 321.
(2) Cramer, S. P.; Stiefel, E. I. In *Molybdenum Enzymes*; Spiro, T. G., Ed.; John Wiley: New York, 1985; p 411.
(3) Stiefel, E. I. *Proc. Natl. Acad. Sci. U.S.A.* **1973**, *70*, 988.
(4) (a) Bray, R. C. *Adv. Enzymol. Rel. Areas Mol. Biol.* **1980**, *51*, 107. (b) Bray, R. C. In *Biological Magnetic Resonance*; Berliner, L. J., Reuben, J., Eds.; Plenum Press: New York, 1980; p 45. (c) Bray, R. C.; Gutteridge, S.; Lamy, M. T.; Wilkinson, T. *Biochem. J.* **1983**, *211*, 227.
(5) (a) Kay, C. L.; Solomonson, L. P.; Barber, M. J. *Biochemistry* **1990**, *29*, 10823. (b) Spence, J. T.; Barber, M. J.; Solomonson, L. P. *Biochem. J.* **1988**, *250*, 921. (c) Spence, J. T.; Barber, M. J.; Siegel, L. M. *Biochemistry* **1982**, *21*, 1656.
(6) For applications of mediator-free CV methods see: Armstrong, F. A. *Struct. Bonding* **1990**, *72*, 137.
(7) Taylor, R. D.; Street, J. P.; Minelli, M.; Spence, J. T. *Inorg. Chem.* **1978**, *17*, 3207.
(8) Spence, J. T.; Minelli, M.; Rice, C. A. In *Molybdenum Chemistry of Biological Significance*; Newton, W. E., Otsuka, S., Eds.; Plenum Press: New York, 1980; p 263.
(9) Subramanian, P.; Spence, J. T.; Ortega, R.; Enemark, J. H. *Inorg. Chem.* **1984**, *23*, 2564.
(10) Dowerah, D.; Spence, J. T.; Singh, R.; Wedd, A. G.; Wilson, G. L.; Farchione, F.; Enemark, J. H.; Kristofzki, J.; Bruck, M. *J. Am. Chem. Soc.* **1987**, *109*, 5655.
(11) Wedd, A. G.; Spence, J. T. *Pure Appl. Chem.* **1990**, *62*, 1055.
(12) Gardner, J. K.; Pariyadath, N.; Corbin, J. L.; Stiefel, E. I. *Inorg. Chem.* **1978**, *17*, 897.
(13) Shriver, D. F.; Drezdzon, M. A. The Manipulation of Air-Sensitive Compounds, 2nd ed.; Wiley-Interscience: New York, 1986.
(14) Perrin, D. D.; Armarego, L. F. *Purification of Laboratory Chemicals*, 3rd ed.; Pergamon Press: Oxford, U.K., 1988.
(15) Bayer, E.; Breitmaier, E. *Chem. Ber.* **1968**, *101*, 1579.
(16) Corbin, J. L.; Work, D. E. *Can. J. Chem.* **1974**, *52*, 1054.

0020-1669/93/1332-1838$04.00/0

Table I. Crystallographic Data and Summary of Data Collection and Refinement Parameters for Compound **1**

empirical formula	$C_{20}H_{26}N_2O_3S_2Mo$
fw	502.5
F_{000}	2064
cryst shape	red plate
temp (°C)	23 ± 3
systematic abs	$h00$, $h = 2n + 1$ $0k0$, $k = 2n + 1$ $00l$, $l = 2n + 1$
cryst system	orthorhombic
space group	$P2_12_12_1$ (Int. Tab. No. 19)
a (pm)	866.7(<1)
b (pm)	1288.4(<1)
c (pm)	1987.7(3)
V (pm^3)	2220×10^6; $Z = 4$
ρ(calc) (g·cm^{-3})	1.504
device	CAD4 (Enraf-Nonius)
wavelength	Cu Kα; λ = 154.18 pm
max scan time (s)	60
scan range (deg)	$1.00 + 0.30 \tan \theta$
max 2θ (deg)	130
reflcns measd	4080; h (−10/10), k (0/15), l (0/23)
indpt reflcns	3162
R(av)	0.023
obsd reflcns ($I > 2.0\sigma(I)$)	2546
structure solution	Patterson method
hydrogen atoms	calcd but not refined
refined params	254
reflcns/param	10.0
R^a	0.056
R(w)^b	0.033
goodness of fit	1.903
residuals (e/Å^3)	+1.26; −0.87
abs corr	empirical
μ (cm^{-1})	136.9
transm coeff	0.335–0.996
extinction	corrected
ϵ	1.140×10^{-7}

^{a} $R = \sum(||F_o| - |F_c||)/\sum|F_o|$. ^{b} $R_w = [\sum w(|F_o| - |F_c|)^2/\sum w|F_o|^2]^{1/2}$ with weighting scheme $(1/\sigma^2(F_o))$.

to 5 mL of a 0.5 M solution of (dmPhb)Zn (2.5 mmol) in DMF. After the mixture was stirred for 15 min, 20 mL of methanol was added and stirring was continued for another 30 min. The solvent was evaporated (50 °C, 0.5 torr). The oily residue was triturated with methanol to give 0.85 g (92%): ^{1}H-NMR (d^6-DMSO, ppm) 3.15 (d, 5.49 Hz, 6 H), 4.10 (q, 5.49 Hz, 2 H), 6.90 (dt, 1.22 Hz, 7.32 Hz, 2 H), 6.98 (dt, 1.22 Hz, 7.33 Hz, 2 H), 7.15 (dt, 1.22 Hz, 7.94 Hz, 2 H) 7.38 (dt, 1.83 Hz, 7.94 Hz, 2 H); ^{13}C-NMR (d^6-DMSO, ppm) 15.82, 59.66, 121.72, 126.25, 126.42, 131.98, 132.23, 141.68; IR (KBr, cm^{-1}) 3346 (ν(N–H)), 751 (δ(CH)).

(mPhabH$_2$)MoO$_2$ was obtained by the metathesis of (mPhabH$_2$)Zn with sodium molybdate. A saturated DMF solution of 0.9 g of (mPhabH$_2$)Zn (2.45 mmol) was combined with 0.62 g of sodium molybdate (2.56 mmol) in an equal volume of water. Complex **1** precipitated upon addition of 5 mL of hydrochloric acid (6 M). It was filtered out and dried over P_4O_{10}. The yield is 0.85 g (81%): ^{1}H-NMR (d^6-acetone, ppm) 1.06 (dd, 73.24 Hz, 7.32 Hz, 6H), 3.44–3.50 (m, 1 H), 3.92–3.99 (m, 1 H), 7.09–7.23 (m, 6 H), 7.37 (d, 7.93 Hz, 1 H), 7.41 (d, 7.93 Hz, 1 H), 8.28 (d, 5.49 Hz, 1 H); ^{13}C-NMR (d^6-DMSO, ppm) 13.98, 15.60, 61.55, 66.85, 125.50, 125.75, 126.32, 126.78, 127.70, 128.21, 128.73, 129.71, 140.19, 142.91, 144.56, 149.14; IR (KBr, cm^{-1}) 3215 (ν(NH)), 912, 902, 878 (ν(Mo=O)), 756, 746 (δ(CH)); EI-MS (m/e): 414 (^{97}Mo; M$^+$ − H$_2$O).

Reductive Deoxygenation of 1. A solution of 176 mg (1 mmol) of methyldiphenylphosphine in 5 mL of DMF was added to 368 mg (0.86 mmol) of (mPhabH$_2$)MoO$_2$ (**1**) and 1 mL (excess) of *N*-methylimidazole in 10 mL of DMF. The solution turned green. Green crystals were formed upon addition of diethyl ether: EPR (THF; 297 K) $\langle g \rangle$ = 1.9869, $\langle A \rangle$ = 3.35 mT; EPR (THF, 253 K) $A_N = 1.85 \times 10^{-4}$ cm^{-1}; EPR (THF, 115 K) $g_\perp$ = 1.980, $g_\parallel$ = 2.005, $A_\perp = 28.7 \times 10^{-4}$ cm^{-1}, $A_\parallel = 52.4 \times 10^{-4}$ cm^{-1}.

Electrochemistry. All experiments were performed on a PAR 173/276 potentiostat (EG&G) using a specially developed CV software program.[17] Cyclic voltammetry (CV) was performed using a three-electrode configuration[18] that consisted of a highly polished glassy carbon disk working electrode (A = 7 mm^2) (Metrohm), a Pt auxiliary electrode, and a Ag/AgCl reference electrode. The working compartment of the electrochemical cell was separated from the reference compartment by a luggin capillary. All compartments contained a 0.1 M solution of tetrabutylammonium hexafluorophosphate (TBAP) (Aldrich) as a supporting electrolyte. All solutions used for the electrochemical experiments were carefully dried, stored under argon, and additionally stirred for more than 1 h over activated alumina. Background CV spectra of the blank electrolyte solution were always recorded. Potentials are reported vs aqueous Ag/AgCl/3 M KCl and have been standardized against ferrocene (THF, 298 K, 0.535 V vs Ag/AgCl; CH_3CN, 296 K, 0.528 V vs Ag/AgCl). For pH adjustments tetramethylammonium hydroxide (Aldrich) in methanol and HCl in ether were used. *N*-Methylimidazole (Aldrich) was dried over molecular sieves and fractionally distilled. Applied scan rates fall in the region between 0.02 and 0.80 V·s^{-1}.

X-ray Crystallography. Crystals of compound **1** were grown from an THF/ether solution. Preliminary examination and data collection were carried out with graphite-monochromated Cu Kα radiation on an Enraf-Nonius CAD4 diffractometer. Crystal dimensions were not determined. Final cell constants were obtained by least-squares refinement of 25 automatically centered reflections at high diffraction angles. Data were collected by $\Theta/2\Theta$ scan mode, and 3 orientation control reflections were monitored every 200 reflections. No change in the intensity of the 3 monitoring reflections could be observed.

The structure was solved by the Patterson method and refined by subsequent full matrix least-squares refinement and difference Fourier electron density maps. Hydrogen atoms were placed at idealized positions and were not refined. The structure also contains one molecule of THF of crystallization per molecule of **1**. Final positional parameters are given in Table II; selected bond lengths and angles are listed in Table III. All calculations were carried out on a MicroVAX 3100 computer in the program system STRUX-IV[19] using the programs SHELXS-86, SDP, PLATON, and ORTEP.

Table II. Final Fractional Atomic Coordinates and Equivalent Isotropic Displacement Parameters for **1** with Estimated Standard Deviations in Parentheses

atom	x/a	y/b	z/c	B_{eq},^{a} (Å^2)
Mo	−0.04117(6)	−0.04899(5)	0.23998(3)	4.44(1)
S(1)	−0.0017(2)	0.0487(2)	0.34321(9)	5.87(6)
S(2)	−0.0428(3)	−0.0991(2)	0.1214(1)	5.49(6)
O(1)	−0.2306(4)	−0.0320(4)	0.2488(3)	5.7(1)
O(2)	0.0066(5)	−0.1726(3)	0.2621(3)	5.5(1)
O(30)	−0.3876(7)	−0.6717(5)	0.3346(4)	12.3(2)
N(1)	0.2241(5)	−0.0098(4)	0.2396(3)	4.0(1)
N(2)	−0.0100(6)	0.1062(4)	0.1804(3)	4.2(2)
C(1)	0.2597(8)	0.0970(6)	0.2157(4)	5.5(2)
C(2)	0.428(1)	0.1082(7)	0.1958(4)	8.6(3)
C(3)	0.1553(8)	0.1155(6)	0.1545(4)	5.3(2)
C(4)	0.183(1)	0.2138(8)	0.1203(5)	9.5(4)
C(11)	0.1869(8)	0.0098(6)	0.3618(3)	4.4(2)
C(12)	0.2801(7)	−0.0221(5)	0.3102(4)	4.5(2)
C(13)	0.4331(7)	−0.0596(6)	0.3228(4)	5.6(2)
C(14)	0.4776(8)	−0.0643(7)	0.3892(4)	7.2(2)
C(15)	0.3910(9)	−0.0285(7)	0.4392(4)	7.0(3)
C(16)	0.2384(9)	0.0062(7)	0.4269(4)	6.6(3)
C(21)	−0.1390(8)	0.0116(6)	0.0931(3)	4.9(2)
C(22)	−0.1201(8)	0.1039(6)	0.1248(4)	4.8(2)
C(23)	−0.2031(9)	0.1933(6)	0.1047(4)	5.7(3)
C(24)	−0.303(1)	0.1847(7)	0.0530(4)	6.4(3)
C(25)	−0.3211(9)	0.0930(7)	0.0179(4)	6.8(3)
C(26)	−0.2383(9)	0.0074(6)	0.0360(4)	5.6(2)
C(31)	−0.313(1)	−0.7636(7)	0.3544(8)	14.0(5)
C(32)	−0.371(2)	−0.7794(9)	0.4154(7)	19.7(6)
C(33)	−0.495(2)	−0.715(1)	0.4271(7)	20.6(5)
C(34)	−0.521(1)	−0.678(1)	0.3639(6)	21.0(5)

^{a} $B_{eq} = {}^4/_3[a^2\beta_{11} + b^2\beta_{22} + c^2\beta_{33}]$.

(17) Amslinger, W. M. Ph.D. Thesis, TU München, Garching, 1991.
(18) Albach, R. W. Ph.D. Thesis, TU München, Garching, 1992.
(19) Kiprof, P.; Scherer, W.; Priermeier, T.; Schmidt, R. E.; Birkhahn, M.; Massa, W.; Herdtweck, E. STRUX-VI, a software program to process X-ray data. Technische Universität München and Universität Marburg, Germany, 1985/1992.

Table III. Selected Bond Lengths (Å) and Angles (deg) for Compound **1**

	Bond Lengths		
Mo–S(1)	2.431(2)	Mo–S(2)	2.444(2)
Mo–O(1)	1.666(4)	Mo–O(2)	1.703(3)
Mo–N(1)	2.355(5)	Mo–N(2)	2.340(5)
	Angles		
S(1)–Mo–S(2)	162.10(7)	S(1)–Mo–O(1)	88.9(2)
S(1)–Mo–O(2)	103.4(1)	S(1)–Mo–N(1)	75.8(1)
S(1)–Mo–N(2)	88.3(1)	S(2)–Mo–O(1)	97.5(2)
S(2)–Mo–O(2)	90.2(2)	S(2)–Mo–N(1)	93.4(1)
S(2)–Mo–N(2)	74.8(1)	O(1)–Mo–O(2)	109.6(2)
O(1)–Mo–N(1)	159.2(2)	O(1)–Mo–N(2)	93.1(2)
O(2)–Mo–N(1)	87.9(2)	O(2)–Mo–N(2)	154.5(2)
N(1)–Mo–N(2)	72.7(2)	Mo–S(1)–C(11)	99.3(3)
Mo–S(2)–C(21)	95.6(3)		

Scheme I

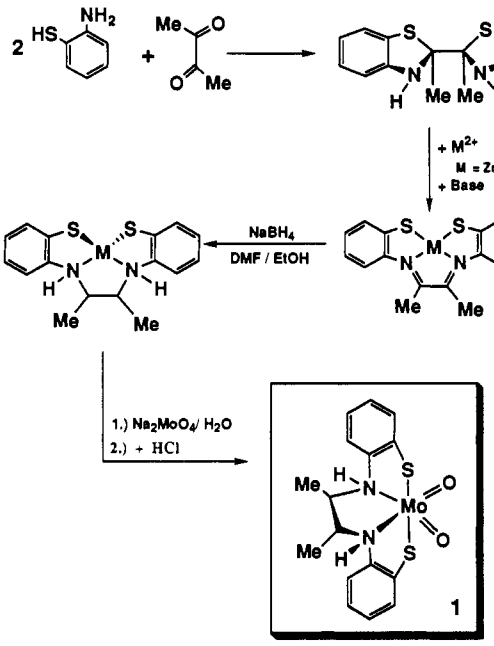

Results and Discussion

(*N*,*N*′-Bis(2-mercaptophenyl)-2,3-diaminobutanato)dioxomolybdenum(VI), (mPhabH$_2$)MoO$_2$ (**1**), has been synthesized using a slightly modified four-step synthesis (Scheme I) via zinc or nickel templates. Complex **1** possesses five chirality centers (one molybdenum center, two nitrogen atoms, and the two carbons of the 2,3-dimethyldiamino group that are substituted by a methyl group). So far, only one diastereomer has been isolated (vide infra).

X-ray Structure of (mPhabH$_2$)MoO$_2$. The chiral complex **1** exhibits a fairly distorted octahedral core geometry with C_2 point symmetry.[20] A view of the structure of the Λ-*S*,*S*,*S*,*S* enantiomer is shown in Figure 1. Selected bond lengths and angles are summarized in Table III. The mononuclear molybdenum(VI) center is in a distorted octahedral environment comprised of two terminal oxo ligands cis to each other, two amine nitrogens trans to the oxo ligands, and two trans-thiolato groups as axial ligands. Similar structures have been described for (mPhaeH$_2$)MoO$_2$[21] (**2**) and (mPhaeMe$_2$)MoO$_2$[10] (**3**) (mPhaeH$_2$ = 2,3-bis(2-mercaptophenyl)diaminoethane, mPhaeMe$_2$ = 2,3-bis(2-mercaptophenyl)-*N*,*N*′-dimethyldiaminoethane). Although the overall structure seems to be similar, bond distances and angles differ significantly.

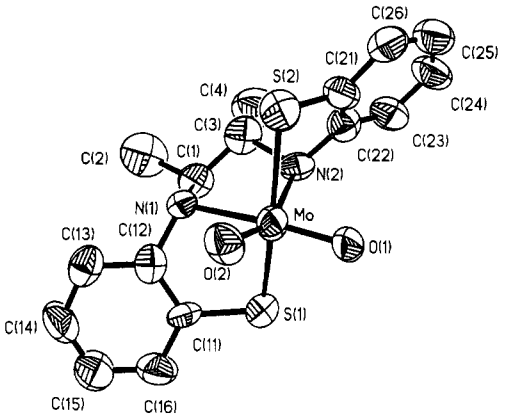

Figure 1. ORTEP drawing of (mPhabH$_2$)MoO$_2$ (**1**).

The Mo–O distances (1.666(4) and 1.703(3) Å) are in the normal range of Mo=O double bonds,[22] and the Mo–S distances are similar to Mo–S single bonds for aromatic thiol ligands.[23] Due to the trans influence of the cis oxo ligands the Mo–N distances are longer than expected for Mo–N single bonds. Presumably because of this effect and the strain in the five-membered ring Mo,N(1),C(1),C(2),N(2) the angle N(1)–Mo–N(2) is much smaller than the ideal value of 90°. A distortion can be noted for the angle S–Mo–S which deviates from ideal linearity but is the closest one to 180° in the series of compounds **1**–**3**.

The strain in the five-membered chelate rings Mo,N(1),C(12),C(11),S(1) and Mo,N(2),C(22),C(21),S(2) finds its expression in the dramatic difference of the N–Mo–S angles within and outside one five-membered ring. The plane defined by the Mo center and the nitrogen ligands is therefore tilted out of the equatorial plane of the octahedron.

Electrochemistry. The electrochemistry under neutral conditions, as first described in DMF[24] and reproduced by us in THF (Figure 2a) and CH$_3$CN, shows one reduction ($E_{pc}(1)$) and two reoxidation steps ($E_{pa}(1)$ and $E_{pa}(2)$), the more anodic of which is quasi-reversible ($E_{pc}(2)$). The peak potentials are summarized in Table IV. According to the peak-current ratio (0.555 ± 0.05)[25] of the primary reduction $E_{pc}(1)$, two electrons are being transferred from the electrode to the complex. These data do not differentiate between a single two-electron transfer and two separate one-electron transfer steps. Below $E_{pc}(1)$ molybdenum is in a tetravalent state. The reoxidations achieve the valence states V and VI, respectively. However, the molybdenum(VI) complex electrochemically produced upon reoxidation is not starting compound **1** but related to it by one chemical step (hydration), as can be shown by analyzing further cycles (Scheme II).

Conjugation of the molybdenum redox orbital to the aromatic π-system increases the reduction potential, as can be shown by comparison with the complex (*N*,*N*′-bis(2-mercapto-2-methylpropyl)ethylendiaminato)dioxomolybdenum(VI). This complex with an aliphatic $S_2(NH)_2$ ligand shows analogous redox chemistry, the irreversible reduction potential being found at −1.41 V (vs Ag/AgCl in DMF at 0.1 V·s^{-1}).[26] Thus the conjugation

(20) Refinement of **1** in the enantiomorphic setting revealed only slight changes in the *R* values to $R = 0.056$ and $R_w = 0.033$ so that it must be assumed that both enantiomers of **1** crystallize in almost equal amounts. Refinement of the enantiomorphic occupation factor was not carried out.

(21) Bruce, A.; Corbin, J. L.; Dahlstrom, P. L.; Hyde, J. R.; Minelli, M.; Stiefel, E. I.; Spence, J. T.; Zubieta, J. *Inorg. Chem.* **1982**, *21*, 917.

(22) Nugent, W. A.; Mayer, J. M. *Metal-Ligand Multiple Bonds*; Wiley: New York, 1988.

(23) Orpen, A. G.; Brammer, L.; Allen, F. H.; Kennard, O.; Watson, D. G.; Taylor, R. *J. Chem. Soc., Dalton Trans.* **1989**, S1.

(24) Spence, J. T.; Minelli, M.; Kroneck, P. *J. Am. Chem. Soc.* **1980**, *102*, 4538.

(25) $i_{rel} = (0.485i_\lambda + i_{pa})i_{pc}^{-1} + 0.086$: Nicholson, R. S. *Anal. Chem.* **1965**, *37*, 1351.

(26) Taylor, R. D.; Street, J. P.; Minelli, M.; Spence, J. T. *Inorg. Chem.* **1978**, *17*, 3207.

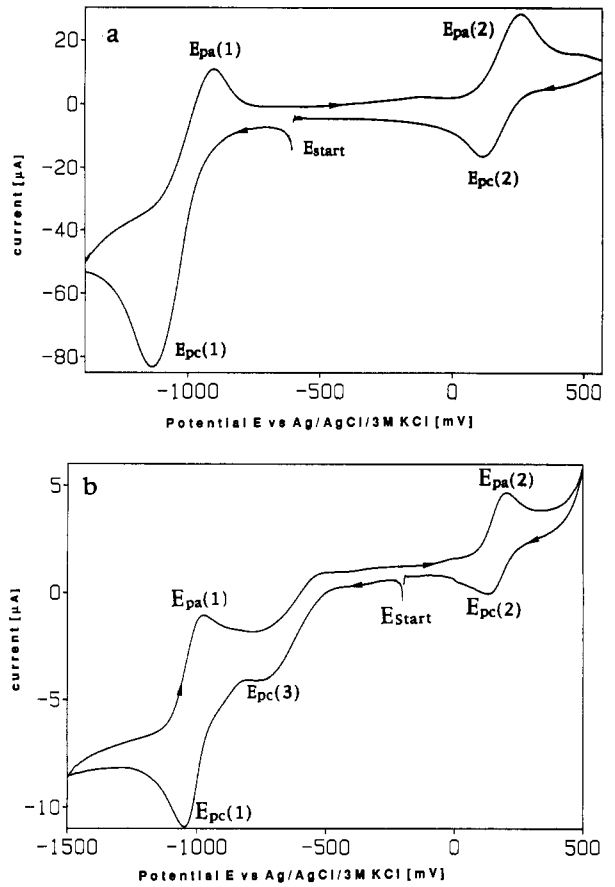

Figure 2. Cyclic voltammograms of $(mPhabH_2)Mo^{VI}O_2$ (**1**) under neutral conditions: (a) in the absence of NMI; (b) in the presence of NMI (56 mmol·L^{-1}). Conditions: 0.1 M Bu_4NPF_6 in THF at 297 K; c_{Mo} = 4.4 mmol·L^{-1}. Scan rates: (a) 200 mV·s^{-1}; (b) 30 mV·s^{-1}.

to a larger π-system is a prerequisite to obtain physiologically accessible potentials.

Addition of *N*-methylimidazole (NMI) to a THF solution of **1** at neutral conditions increases the first one-electron reduction potential of $(mPhabH_2)MoO_2$. This effect depends on the concentration of the nucleophile. For low concentrations (21 mM) a shoulder appears on the anodic side of the reduction wave. For higher concentrations (56 mM) two peaks of equal height ($E_{pc}(3)$ and $E_{pc}(1)$) can be discerned, each corresponding to a one-electron reduction (Figure 2b). Therefore, addition of the nucleophile NMI allows us to propose a mechanism for the electrochemically induced reactions of **1** that clearly involves two separate one-electron reduction steps (Scheme II). The first, being irreversible ($E_{pc}(3)$), leads to an unstable Mo(V) intermediate, which readily undergoes dehydration to form the known Mo(V) monoanion $[(mPhab)MoO]^-$ (**4**).[24] Most likely, this EC mechanism proceeds via an initial protonation reaction followed by NMI coordination. The second wave ($E_{pc}(1)$) which is quasi-reversible resembles the reduction of **4** to the dianion $[(mPhab)MoO]^{2-}$. The reason for the separation of the two redox processes upon addition of NMI can be explained by the dependence of the peak potential upon the rate of the subsequent dehydration reaction.[27] In the presence of NMI, the rate of this dehydration reaction decreases by a factor of 10, as estimated from theoretical models.[28]

Acidic conditions, obtained by adding 1 M HCl in ether to the solution of **1**, give a CV (Figure 3) similar to that obtained by adding NMI (Figure 2b). Two separate reduction waves are observed, each accounting for a one-electron reduction and each

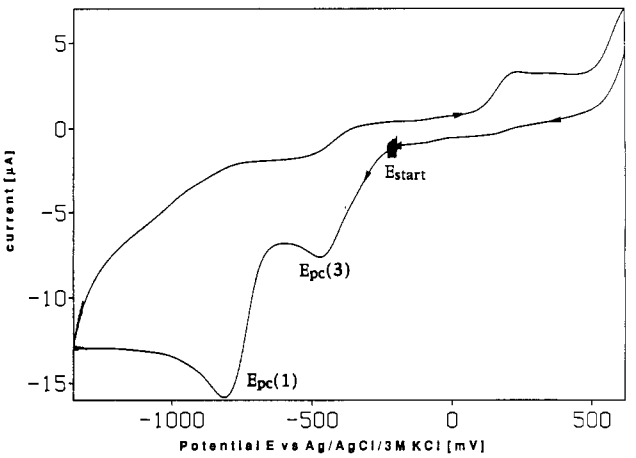

Figure 3. Cyclic voltammogram of $(mPhabH_2)Mo^{VI}O_2$ (**1**) under acidic conditions: HCl in ether (6.8 mmol·L^{-1}); 0.1 M Bu_4NPF_6 in THF at 295 K; c_{Mo} = 4 mmol·L^{-1}; scan rate 20 mV·s^{-1}.

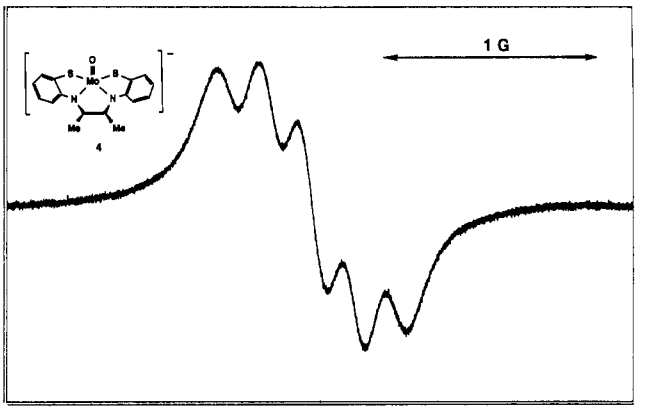

Figure 4. EPR spectrum of **4** (253 K) in THF/CH_3OH. Only the central line (I_{Mo} = 0; $\langle g \rangle$ = 1.9852) is shown (A_N = 1.85 × 10^{-4} cm^{-1}).

being irreversible. As expected for such an ECE process,[28] the normalized peak current $i_{pc}\cdot v^{-1/2}$ decreases with increasing scan rates v.

At low proton concentrations, as at low NMI concentration, the first reduction is visible only at slow scan rates ($E_{pc}(3)$ = –0.46 V; v = 0.02 V·s^{-1}) due to the scan rate dependence of the irreversible peak potentials. In the case of higher proton concentrations, $E_{pc}(3)$ (–0.516 V; v = 0.8 V·s^{-1}) is discernible at all scan rates. The irreversible wave can be assigned to the formation of an intermediate as seen upon addition of NMI. Such species have been characterized in the case of analogous N-alkylated ligand systems.[10] Protons accelerate the formation of the intermediate, but its subsequent dehydration to **4** is retarded by protons. The peak potential $E_{pc}(1)$ (Mo^{V}/Mo^{IV}) increases with increasing proton concentration as expected for an ECEC mechanism.[28] The dianion $[(mPhab)Mo^{IV}O]^{2-}$ formed in the second reduction step reacts with protons to form some yet unidentified product.

Upon addition of tetraethylammonium hydroxide in methanol the formerly orange solution (neutral pH) immediately turns green. Reduction of **1** and quantitative formation of $[(mPhab)MoO]^-$ (**4**) takes place. The EPR spectrum of **4** (Figure 4) shows superhyperfine coupling to both amido ligands (A_N = 1.85 × 10^{-4} cm^{-1}) as previously demonstrated for similar complexes.[29] In contrast to the neutral and acidic conditions, the voltammetric cycles start at the Mo(V) state and therefore differ. The first reduction step ($E_{pc}(1)$) has a quasi-reversible counterpart $E_{pa}(1)$. The half-wave potential of this quasi-reversible wave ($\alpha\cdot n_\alpha = 2.2E_{th}(\Delta E^{-1}) = 0.47 \pm 0.05$; $E_{th} = RTF^{-1}$ = 25.59 mV)

(27) Nicholson, R. S.; Shain, I. *Anal. Chem.* **1964**, *36*, 706.
(28) Heinze, J. *Angew. Chem., Int. Ed. Engl.* **1984**, *23*, 831.
(29) Rajan, O. A.; Spence, J. T.; Leman, C.; Minelli, M.; Sato, M.; Enemark, J. H.; Kroneck, P. M. H.; Sulger, K. *Inorg. Chem.* **1983**, *22*, 3065.

Scheme II

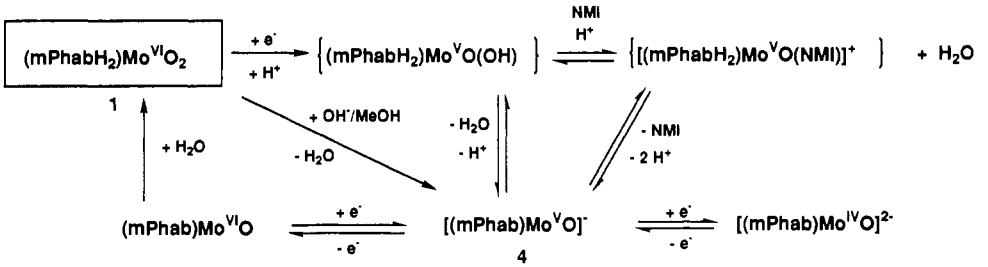

Table IV. Cyclovoltammetric Parameters for **1** under Various pH Conditions

	neutral[a]				neutral with NMI[b]					acidic[c]		basic[d]			
	$E_{pc}(1)$	$E_{pa}(1)$	$E_{pa}(2)$	$E_{pc}(2)$	$E_{pc}(3)$	$E_{pc}(1)$	$E_{pa}(1)$	$E_{pa}(2)$	$E_{pc}(2)$	$E_{pc}(3)$	$E_{pc}(1)$	$E_{pc}(1)$	$E_{pa}(1)$	$E_{pa}(3)$	$E_{pa}(2)$
C_E[e] (V)	−1.24	−0.88	0.30	0.09	−0.774	−1.13	−0.96	0.215	0.127	−0.52	−1.034	−1.042	−0.894	0.052	0.02
m_E[e] (V)	−0.11	−0.025	−0.05	−0.038	−0.034	−0.024	0.013	0.008	0.006	−0.043	−0.054	−0.019	0.013	−0.092	−0.033
i_{rel}[f]	0.525		0.879		0.98			0.66		irreversible		1.0		irreversible	

[a] 4.44 mmol·L^{-1} of **1** in THF/0.1 M TBAP at 297 K. [b] 4.4 mmol·L^{-1} of **1** and 56 mmol·L^{-1} NMI in THF/0.1 M TBAP at 297 K. [c] 4 mmol·L^{-1} **1** in THF/0.1 M TBAP and 6.8 mmol·L^{-1} HCl in ether at 295 K. [d] 4 mmol·L^{-1} **1** in THF/0.1 M TBAP and 12 mmol·L^{-1} Et_4NOH in MeOH at 297 K. [e] Where $E_{px}(n) = C_E + m_E \log v$ (vs Ag/AgCl). [f] i_{rel}[26] at a scan rate of 200 mV·s^{-1}; experimental error ±0.05.

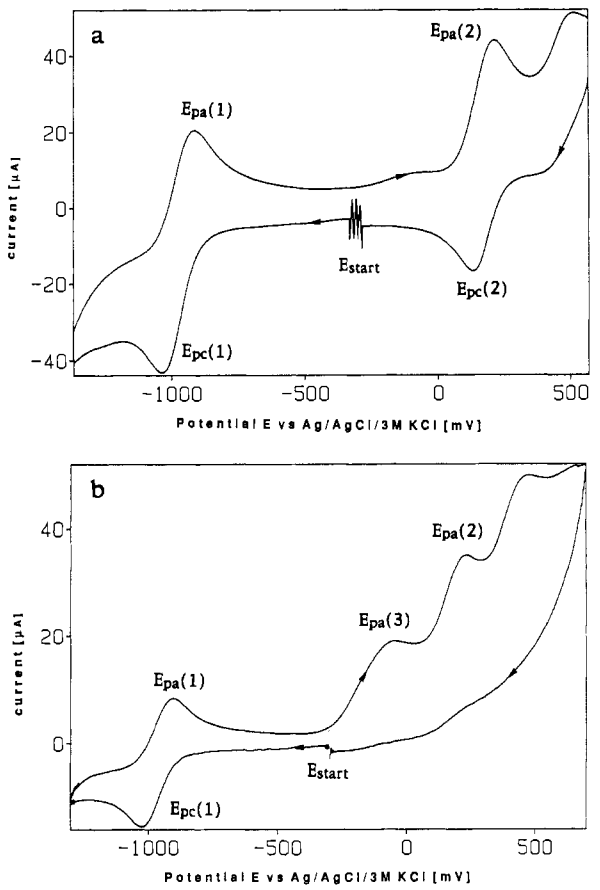

Figure 5. Cyclic voltammograms of $(mPhabH_2)Mo^{VI}O_2$ (**1**) under basic conditions: Et_4NOH/MeOH (a, 3 mmol·L^{-1}; b, 12 mmol·L^{-1}); 0.1 M Bu_4NPF_6 in THF at 297 K; c_{Mo} = 4 mmol·L^{-1}. Scan rates: (a) 800 mV·s^{-1}; (b) 200 mV·s^{-1}.

is found at −0.970 V vs Ag/AgCl/3 M KCl in THF/0.1 M $[(C_4H_9)_4N]PF_6$. The peak–current ratio (1.01 ± 0.05) supports the interpretation as a one-electron transfer to form the Mo(IV) dianion. At low tetraethylammonium hydroxide concentration (3 mM) a second quasi-reversible wave is observed ($E_{pa}(2)/E_{pc}(2)$) which can be assigned to the electrochemical oxidation of **4** to $(mPhab)Mo^{VI}O$ (Figure 5a). However, upon increase of the hydroxide concentration the oxidation wave becomes irreversible due to the accelerated hydration reaction of $(mPhab)Mo^{VI}O$

Scheme III

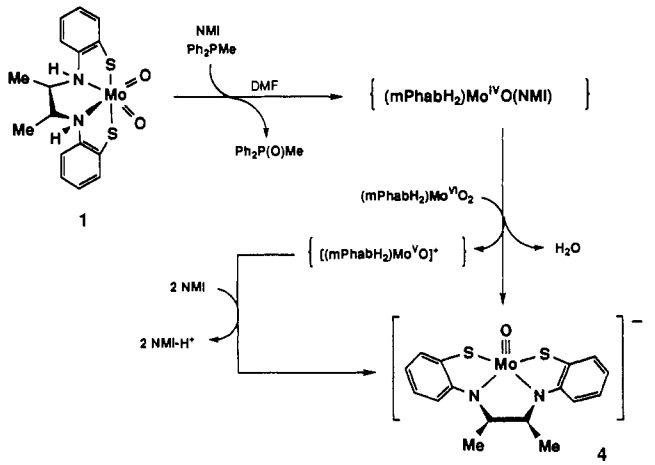

(Figure 5b). In addition, a second irreversible oxidation step ($E_{pa}(3)$) appears at a slightly lower potential.

Deoxygenation Reactions. Oxygen atom transfer reactions of the MoO_2^{2+} fragment using phosphines are known to yield mononuclear Mo(IV) complexes in some cases.[30] However, upon addition of Ph_2PMe in DMF to the Mo(VI) complex **1** only a black-brown powder that lacks terminal oxo functions is obtained. Dehydration reactions seem to play a major role in the chemistry of **1**. Suppression of such a reaction pathway can either be achieved by using ligands containing no amino protons (complete N-alkylation)[31] or by stabilization of the Mo(IV) oxo-transfer product. We therefore reacted **1** with methyldiphenylphosphine in DMF using an excess of *N*-methylimidazole. Within minutes the reaction mixture turned green. Neither μ-oxo–Mo^V–Mo^V dimers nor Mo(IV) monooxo complexes could be isolated. Only methyldiphenylphosphine oxide and a green Mo(V) monooxo species were obtained. As shown by EPR (nitrogen superhyperfine coupling), $[(mPhab)MoO]^-$ (**4**) is formed in quantitative yield. NMI, an excellent nucleophile, seems to be important for the observed reaction pathways.

We propose that coordination of NMI shifts the oxidation potential of the Mo(IV) complex above the reduction potential of **1** to allow comproportionation between the molecules (Scheme III). Subsequent dehydration yields Mo(V)–monooxo monomers. Interestingly, no μ-oxo-dimer formation can be observed as

(30) Holm, R. H. *Chem. Rev.* **1987**, *87*, 1401.
(31) Boyd, I. W.; Spence, J. T. *Inorg. Chem.* **1982**, *21*, 1602.

expected for such systems.[31] Finally, deprotonation of the Mo(V) species yields [(mPhab)MoO]$^-$ (**4**). Other nucleophiles such as tetrahydrothiophene or DMF do not stabilize the highly reactive Mo(IV) intermediates. As a result, further dehydration occurs leading to completely deoxygenated Mo species.

Conclusion

Electrochemistry of the investigated Mo(VI) dioxo complex clearly shows that variations in the local proton concentrations have a major influence on the electrochemistry of such systems. Not only is a dependency of the potentials on the proton concentration observed but, even more important, different subsequent chemical reaction pathways become possible. In contrast to earlier reports, the molybdenum(V) state seems to be an electrochemically observable intermediate, even in so-called two-electron transfer steps of MoO_2^{2+} species.

Deprotonation of the ligands surrounding the Mo site strongly influences the reaction pathways upon reduction. Oxygen atom transfer using phosphines yields $Mo^{IV}O^{2+}$ species starting from molybdenum(VI) dioxo complexes only with nondeprotonatable ligands. In contrast, complexes such as **1** allow deprotonation and lead to Mo(V) species upon phosphine reduction via a dehydration process. Electrochemical reductions allow reversible one-electron transfer in the cases of Mo(VI) dioxo compounds with nondeprotonatable ligands. Analogous complexes with deprotonatable ligands favor dehydration upon one-electron reduction, thus leading to an irreversible electron-transfer step. However, further one-electron reduction of those complexes under electrochemical conditions yields stable Mo(IV) dianions. Preparative synthesis of such species is in progress. We therefore propose a major influence of surrounding groups (local pH, deprotonatable/nondeprotonatable) at the active site of molybdoenzymes on the redox reaction pathway (oxo transfer vs electron/proton transfer).

Acknowledgment. The authors thank Prof. Enemark for critical discussion. Financial support of this work by the Fonds der Chemischen Industrie (fellowship for R.W.A.) and the Deutsche Forschungsgemeinschaft is gratefully acknowledged.

Supplementary Material Available: Tables of atom positions, anisotropic displacement parameters, and bond distances and angles for all atoms (7 pages). Ordering information is given on any current masthead page.